Colloidal suspensions of monodisperse diamond core-shells

A Venerosy, Hugues Girard, Samuel Saada, Mohamed Sennour, I Stenger, M. Mermoux, Jean-Charles Arnault

Colloidal Suspensions of Monodisperse Diamond Core-Shells

A. Venerosy[1], H. A. Girard[1], S. Saada[1], M. Sennour[2], I. Stenger[3], M. Mermoux[4], J. C. Arnault[1*]

[1] CEA, LIST, Diamond Sensors Laboratory, 91191 Gif-sur-Yvette, France
[2] Centre d'Etudes de Chimie Metallurgique, UPR 2801 CNRS, F-94407 Vitry sur Seine, France
[3] Groupe d'Etude de la Matière Condensée, Université de Versailles St Quentin, CNRS, Université Paris-Saclay, 45 avenue des Etats-Unis, 78035 Versailles cedex, France
[4] Univ. Grenoble Alpes, Univ. Savoie Mont Blanc, CNRS, Grenoble INP, LEPMI, 38000 Grenoble, France

*Corresponding Author E-mail address: jean-charles.arnault@cea.fr

Abstract

We report on an innovative method to synthesize monodispersed diamond core-shells stable in colloidal aqueous suspensions. Starting with an electrostatic seeding of silica particles by detonation nanodiamonds, carefully driven in terms of charge and proportion, we are able to initiate the growth of a carbon coating all around the seeded silica particles in a plasma MPCVD reactor dedicated to powder treatments. The crystalline structure of the carbon coating can be tuned by changing the MPCVD conditions: from nanocrystalline diamond for low methane content to graphite nanoflakes for high methane content. These materials are characterized by FE-SEM, HR-TEM, FTIR and Raman spectroscopy. Preliminary photoluminescence (PL) data are also provided. A chemical post-treatment of the core-shell particles is applied to obtain colloidal stability in neutral aqueous suspensions. The monodispersity and the colloidal stability are assessed using DLS and Zeta measurements. After the removal of the silica core, stable suspensions of diamond hollow spheres are obtained. This new class of diamond-based material may find promising applications in various fields, such as nanomedicine toward a versatile nanotool for drug delivery or biolabeling, catalysis thanks to its controllable porosity and carbon surface chemistry or photonics as an elemental block toward bottom-up ordered diamond structures.

Keywords : Diamond, Shell, Chemical Vapor Deposition, Nanocrystalline

1. Introduction

Nanodiamonds (NDs) possess outstanding chemical and physical properties useful for various applications fields. Their primary size can be tuned from few nm (2-7 nm for detonation [1]) to tens or hundreds of nm (for NDs milled from high pressure and high temperature (HPHT) synthetic diamond [2]). NDs have properties rather similar to bulk diamond, such as e.g. exceptional hardness, room temperature luminescence [3] and even biocompatibility [4]. The fine control of their surface chemistry allows either the synthesis of stable colloids [5] or their functionalization with complex molecules [6]. This motivates their use in composites [7], biology for therapy or diagnosis [1,8] or for electrochemistry [9]. However, diamond nanoparticles are facing some drawbacks, which can limit their development and their use, such as their shape and polydispersity. For example, sub-10 nm nanoparticles produced by detonation synthesis easily tend to strongly aggregate in colloidal suspension into polydispersed clusters of few particles [10], difficult to precisely control in terms of overall size and shape. At the opposite, nanoparticles produced by milling techniques are less sensitive to aggregation and can be easily stabilized at their primary size. However, as a consequence of their synthesis, they are constituted of highly polydispersed faceted fragments which are difficult to sort [11]. Indeed, these two aspects can have major impacts on biological behaviors of nanodiamonds, especially on their cell internalization [12]. Another disadvantage is the lack of sphericity of the available diamond particles, whether in the form of clusters or fragments, which prevents them from almost any promising applications using self-assemblies.

Several attempts were previously reported to overcome the present limitations of NDs in terms of polydispersity and sphericity. For example, Cigler's team reported on a surface treatment to get rounded HPHT NDs via an annealing in melted KNO_3 [13]. Nevertheless, these rounded NDs remain polydispersed as synthesized from milled ones[12]. The same group also proposed a core-shell system to obtain a better sphericity of their nanodiamonds, the core being the diamond nanoparticles and the shell a fine silica coating [12]. Another approach used detonation NDs to decorate droplets in an emulsion, so-called diamondosomes. However, these structures are highly fragile and can easily collapse under solvent strength [14]. Diamond microspheres were also obtained by scratching process on substrate as shown by Q. Wang et al. [15]. Another strategy was based on the use of a hard spherical and sacrificial template to synthesis hollow carbon spheres [16]. Silica template with different shapes (spheres, fibers) can be also used to graft NDs on their surfaces [17]. Silica templates were also used as hard templates to grow diamond on them, as reported several times in the literature. For instance, the team of John et al. coated silica particles of 25 µm up to 200 µm diameter deposited on a copper substrate with a thick diamond layer (1 µm) [18,19]. A similar approach was used by Nebel's team to fabricate boron doped diamond foams from silica particles seeded with NDs and grown successively on a silicon wafer through a layer-by-layer approach, toward electrochemical applications [20].

In the present paper, we aim to synthesize monodispersed and spherical micrometric diamond core-shell structures, as well as diamond hollow spheres, able to be dispersed in colloidal suspensions and used as any other core-shell systems. Conventional diamond Microwave Plasma Chemical Vapor Deposition (MPCVD) growth on silica particles deposited on a silicon wafer is not suitable for this purpose. Indeed, a simple calculation shows that theoretically less than 2 mg of coated silica spheres can be produced from a 2 inches silicon wafer covered with a monolayer of silica particles (1µm of diameter), spaced by 500 nm, without taking into account the loss due to the experimental manipulations. We therefore developed another synthesis route based on a MPCVD diamond growth directly performed on micrometric or sub-micrometric particles in a powder form. For this, we first adapted a seeding technique which proved to be able to deposit a monolayer of 5 nm NDs at the surface of silica particles, directly in aqueous suspension [21]. Then, we applied diamond MPCVD growth on seeded SiO_2 particles using a home-made reactor specifically designed for powder treatments. This set-up was subsequently optimized to ensure the monodispersity of the resulting material. Dealing with their surface chemistry, we provided to the coated particles a negative surface charge to ensure their colloidal stability. The morphology of these materials was first investigated by field emission scanning electron microscopy (FE-SEM). Surface modifications and crystalline microstructure of both materials were then carefully characterized using Fourier Transformed Infrared Spectroscopy (FTIR), High Resolution Transmission Electron Microscopy (HR-TEM), Raman and photoluminescence (PL) spectroscopies.

In addition, based on this combination of characterization techniques, we demonstrate that the crystalline structure of the carbon coating covering the silica particles can be tuned from nanocrystalline diamond to graphitic nanoflakes depending on MPCVD conditions. Hollow spheres of these two materials were used to prepare stable colloidal aqueous suspensions.

2. Experimental

2.1 Materials

Potassium hydroxide, sodium hydroxide, potassium bromide and silica particles (1 µm in size suspended in water) were purchased from Sigma-Aldrich. Hydroxylated 5 nm detonation nanodiamond positively charged in aqueous suspension were bought from Adamas Nanotechnology. All these chemicals were used as received.

2.2 Seeding of SiO_2 templates

To perform the seeding of SiO_2 particles with NDs, initial solutions at 10 mg/mL for SiO_2 and 1 mg/mL for NDs were used. Different concentration ratios of NDs/SiO_2 were tested (see Table 1). Ratios were investigated to be theoretically above or below the ideal density of 10^{12} particles/cm² and had to be accurately controlled to avoid (i) an uncompleted coverage of the NDs on the SiO_2 particles or (ii) an excess of NDs in the SiO_2 particles suspension, which would result in an inhomogeneous diamond coating of the silica particles. These solutions were stirred for 10 min, leading to the electrostatic grafting of the NDs on the silica particles [22]. To produce carbon coated silica particles in a sufficient amount (tens of mg), it is necessary to dry them. These mixtures were dehydrated in a heat chamber at 60°C to obtain a powder of seeded particles.

Table 1: Solutions with different concentration NDs/SiO_2 ratios.

Name	Concentration ratios NDs/SiO_2 (%)
A	0.1
B	1.4
C	13.8

2.3 MPCVD (Microwave Plasma - Chemical Vapor Deposition) growth conditions

CVD diamond growth on seeded SiO_2 particles was performed using a home-made reactor dedicated to powder treatments [20][24]. 10 mg of dried silica particles coated with NDs were introduced in a quartz tube. The tube was then pumped to a primary vacuum level (~10^{-3} mbar). For all experiments, methane (CH_4) and hydrogen (H_2) gases were injected up to 12.5 mbar, using different CH_4/H_2 ratios and growth duration at a total flow of 10 sccm.

In a first study (part 3.1), CH_4 concentration was kept constant to 2 vol. % in H_2 and different deposition times were used: 10, 20, 30, 50 and 60 min. The CH_4/H_2 ratio is known to strongly govern the crystalline quality of the carbon coating. Therefore, in a second study (part 3.3), different CH_4/H_2 ratios were used: 2 %, 5 %, 10 % and 30 %. The growth duration was fixed at 1 hour, except for the highest methane content (30 %) for which it was reduced to 45 min. For all these experiments, the plasma was generated in the quartz tube using a microwave power at a frequency of 2.45 GHz. The geometry of the home-made reactor prevents the measurement of the temperature during the growth inside the tube.

2.4 Photochemical oxidation of coated particles

After the CVD growth, coated SiO_2 particles were dried and oxidized through a photochemical treatment under ozone to confer a hydrophilic behavior to the material [25]. During the process, coated particles were exposed to UV light using a Xenon excimer lamp (wavelength 172 nm) under a low pressure of ozone (300 mbar) in an alumina crucible.

2.5 Preparation of colloidal particles suspensions

Oxidized coated particles were then dispersed in water by sonication (Hielscher UP400S, 400 W, 24 kHz at 40% and 0.5 cycles) during 2min.

2.6 Preparation of spheres

To obtain hollow spheres, silica cores were dissolved in a boiling Murakami solution (NaOH 1.2 mol/L and KOH 8.9 mol/L) for 10 min. Shells were then washed by successive sedimentation/rinsing cycles with deionized water until a neutral pH was reached.

2.7 Characterization methods

SEM analysis (Scanning Electron Microscopy). The surface topography of samples deposited on silicon wafers was observed by field emission scanning electron microscopy (FE-SEM) performed with a Supra® 40 microscope (from Carl Zeiss in Germany). By using an Inlens detector, a high lateral resolution of approximately 5 nm was obtained. SEM images were obtained at a working distance

(WD) range between 2.0 and 2.5 mm and using an acceleration voltage in range 1-20 kV. To observe particles by FE-SEM, a drop of solution of them was deposited on silicon substrate.

Dynamic Light Scattering (DLS) and Zeta Potential (ZP) measurements. The hydrodynamic size and ZP measurements of SiO_2 templates, coated SiO_2 core-shells and shells suspensions were performed in ultrapure water on DLS (Nanosizer ZS, Malvern). Hydrodynamic size and zeta potential analysis were measured with a 633 nm laser at 25 °C at a scattering angle of 173°.

FTIR (Fourier Transform InfraRed) spectroscopy. Spectra were measured in a transmission mode using a FTIR spectrometer (Nicolet™ 8700, Thermo scientific). 150 mg KBr pellets were prepared with few mg of samples.

Raman spectroscopy. Samples were examined at different excitation wavelengths. Raman measurements were performed using two different instruments. The first was a monochromator spectrometer (T64000 triple, Jobin-Yvon) that allowed measurements in both visible and UV spectral ranges. For this purpose, it was equipped with a UV-enhanced liquid-nitrogen-cooled CCD detector, a microscope, two different confocal optics, and interchangeable gratings (2400, 1800, 1200 and 600 grooves/mm). The second instrument was a spectrometer (InVia™, Renishaw) that allowed measurements in the visible, near-UV, and near-IR spectral ranges. It is equipped with an air-cooled CCD detector and a microscope. For all instruments, a 50x (numerical aperture or NA = 0.85) objective and a UV-dedicated 40x (NA = 0.5) objective were used to focus the laser on the sample surface and collect the scattered light. Three different excitation wavelengths were used: the 514 nm line of an Argon laser, the 532 nm line of a frequency-double YAG laser and the 325 nm line of He-Cd laser. The T64000 instrument was also used for the acquisition of the preliminary photoluminescence data presented in the following. PL data were not corrected for the instrument response. Incident powers, typically a few mW, were adapted to avoid any strong heating of the samples.

HR-TEM (High-resolution Transmission electron Microscopy). Observations were made by using a HR-TEM (F20 FEI 200kV, Tecnai) at 200 keV and equipped with a Gatan Imaging Filter. A high lateral resolution of 2.3 Å was obtained. Samples were deposited on a 3 mm diameter cooper grid covered with a holey carbon film by manual dip coating. Images were performed near Scherzer focalization (−63 nm) using a (1 k × 1 k) charge-coupled device camera. Local area fast Fourier transform diffractograms, equivalent to electron diffraction patterns, were exploited to determine structural and crystallographic characteristics of the observed samples.

3. Results and discussion

3.1 Optimization and control of nanodiamond seeding on silica core

Silica particles, as received and seeded with three concentration ratios of NDs/SiO_2 (Table 1), were observed by FE-SEM. Images are provided in Figure 1(a-d). Particles seeded with the lowest amount of NDs (solution A) exhibit a rather low surface coverage which can be substantially improved (Figure 1b). The SEM image also shows a negligible aggregation of NDs on silica particles. Figure 1c shows particles seeded with a ten times higher amount of NDs (solution B), revealing a more regular coating. For the highest amount of NDs (Solution C, Figure 1d), the SEM image shows a full coverage of NDs on silica surface. However, some excess of NDs is clearly visible, leading to bridges between particles. This may favor the coalescence of particles during the MPCVD growth. As a consequence, the ratio of NDs/SiO_2 corresponding to the solution B was further used for all samples. Note that despite the high resolution of the FE-SEM used here, the calculation of the experimental density of seeds from image analysis remains difficult, partly due to the insulating behavior of SiO_2 particles which induces a charging effect.

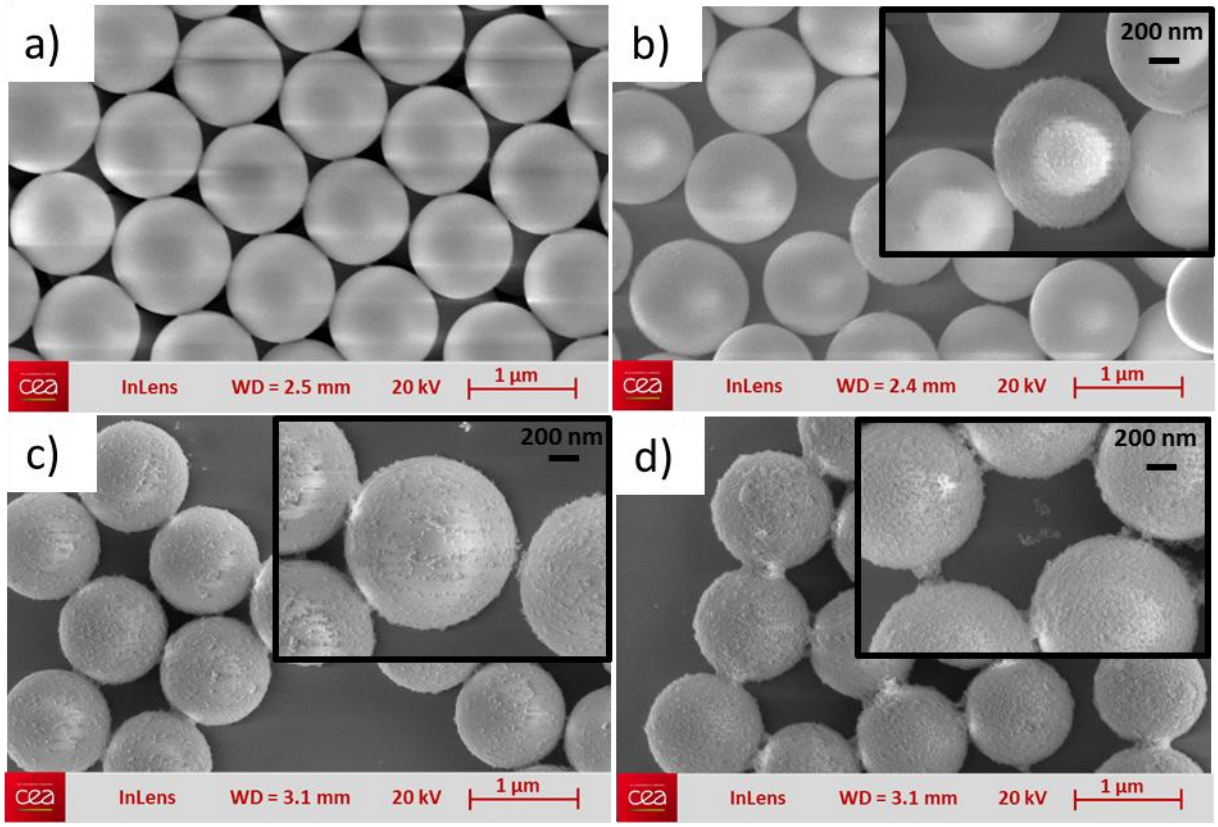

Figure 1: SEM images of a) as received SiO_2 particles compared to SiO_2 particles seeded with different NDs/SiO_2 ratios (see Table 1); b) 0.1%; c) 1.4%; and d) 13.8%.

Prior to the MPCVD growth, the suspension of seeded silica particles was dried to recover a powder state. The annealing was performed at 60°C. To check the NDs adhesion after drying step, a small amount of powder was re-dispersed in water and subsequently observed by SEM (not shown). Very similar images were acquired with NDs still present on SiO_2 surface after the drying step. Therefore, the thermal treatment has no effect on seeds, which confirms the strong adherence of the NDs on silica particles.

3.2 Synthesis and characterization of diamond shells

SEM images of seeded SiO_2 particles grown with 2 % vol. CH_4 in H_2 for different times (10 min to 60 min) are compared in Figure 2. Whatever the growth time, a coating is observed on silica particles, made of small grains with diameters around few tens of nanometers. This coating remains very similar to nanocrystalline diamond layers (confirmation given by HRTEM in Figure 8). At the same time, an increase of the coating thickness with growth time is also noticed, as shown in Figure 2 and summarized in Figure 3. A linear trend is obtained for deposition times lower than 30 min while a reduction of the slope is observed for longer durations, which could be related to lateral stresses induced by the spherical shape of silica template. Finally, we can also highlight that some of the silica particles remains uncoated. This inhomogeneity between the particles is likely due to the geometry of the powder-dedicated CVD reactor which still needs to be optimized.

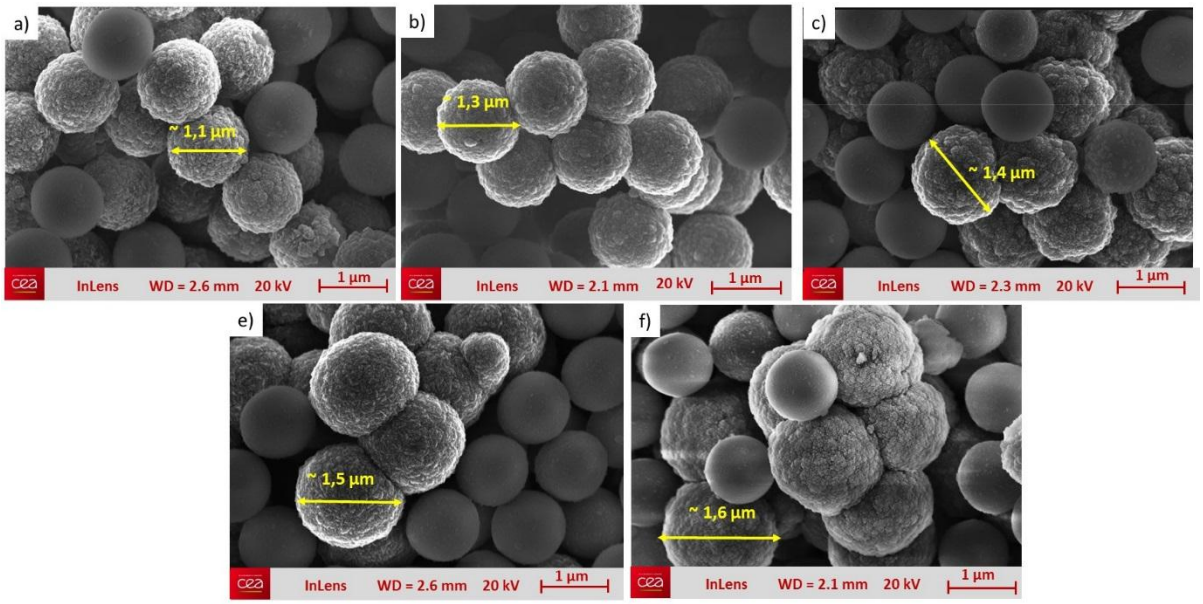

Figure 2: Morphology of silica particles seeded with NDs after MPCVD growth at 2 % of methane for different deposition times a) 10 min, b) 20 min, c) 30 min, d) 50 min and e) 60 min. Other MPCVD parameters: total pressure 12.5 mbar, flow rate 10 sccm, microwave power 180 W. Yellow arrows indicate the diameter of coated particles.

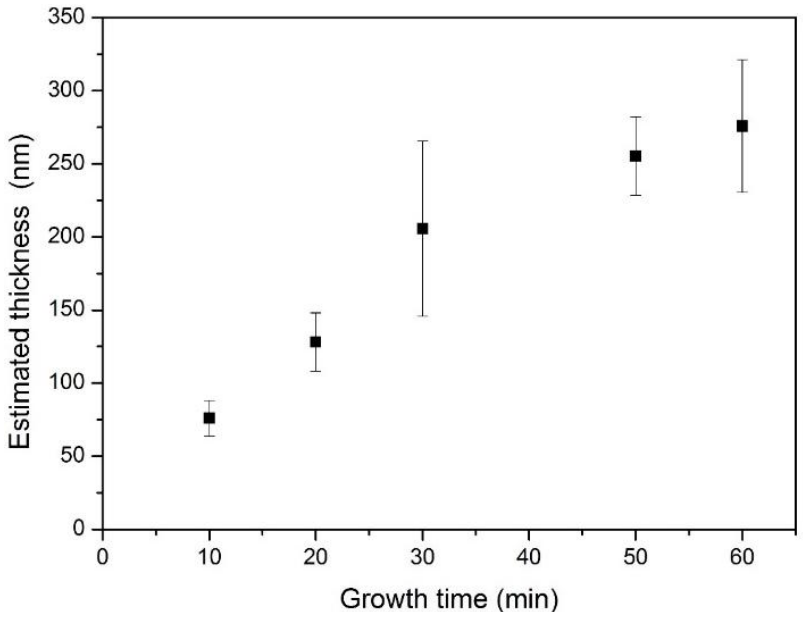

Figure 3 : Evolution of the coating thickness with MPCVD deposition time for 2 % of methane. Error bars represent experimental standard deviations on the coating thickness considering 5 particles on SEM pictures.

A full coverage of silica particles is achieved after 10 min of MPCVD deposition at 2% of methane (Figure 3a), while preserving a spherical shape with limited connections between coated particles. Thus, these structures grown for 10 min were chosen as the most appropriate material to further obtain isolated coated particles in colloidal suspension.

After the MPCVD growth, particles were poured in deionized water. Part of them exhibit a hydrophobic behavior and float over the water surface (Figure 4a), in agreement with properties of hydrogenated diamond surface known to be highly hydrophobic [26]. The other part of the treated silica particles immediately drops at the vial bottom, being composed of heavy aggregates (coated or uncoated) and the uncoated silica particles seen in Figure 2. Therefore, only the hydrophobic particles were extracted to keep only isolated or slightly aggregated coated silica particles. After drying, an oxidation treatment was performed by a UV exposure (λ=172 nm) under 300 mbar of ozone for 2 h to confer a hydrophilic surface. After being put in water, a short sonication step was applied to promote the separation of slightly coalesced coated particles. Using this procedure, a stable suspension was obtained (Figure 4b).

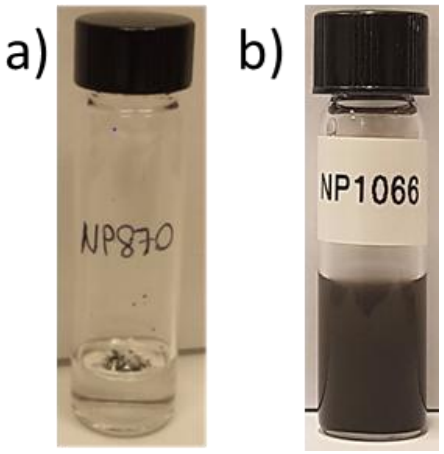

Figure 4: Colloidal aqueous suspensions of a) hydrophobic coated particles after MPCVD growth and b) hydrophilic oxidized coated particles after UV exposure.

Colloidal properties of the later suspension were investigated using Dynamic Light Scattering (DLS). Hydrodynamic diameter in aqueous suspension of as received and diamond coated silica particles are compared in Figure 5. The hydrodynamic diameter was estimated to 1243 nm for as received silica particles. For the oxidized diamond core-shells, two peaks were detected, the main one at 1259 nm and the second at 5317 nm which obviously corresponds to some aggregated particles in a very limited amount according to the low intensity of their scattered light. The DLS spectrum shows a narrow size distribution for both colloids, meaning that after the MPCVD growth, the monodispersity of particles is preserved. As received silica particles possess a negative zeta potential (ZP) of - 84 mV. After diamond coating and surface oxidation, core-shells exhibit a ZP of - 44 mV, which still guarantees a colloidal stability. This negative value is in agreement with an oxidized surface chemistry for diamond coated particles, as already reported for nanodiamonds [6]. Finally, hydrophilic diamond coated particles could be easily dispersed in aqueous solutions.

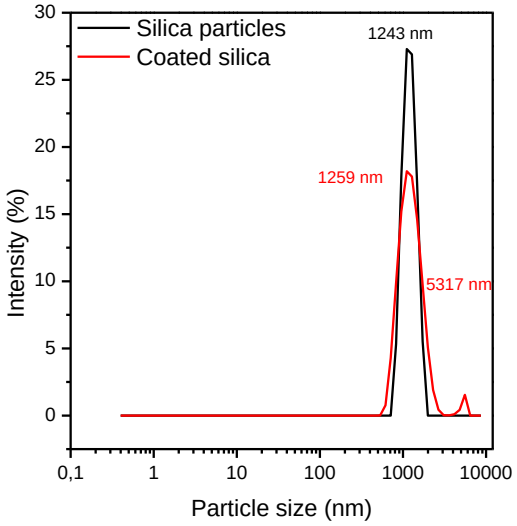

Figure 5 : Distributions of hydrodynamic diameter for as received silica particles (in black) and oxidized coated silica particles (in red).

After the MPCVD growth, the SiO_2 template can be removed by a wet chemical treatment. The complete dissolution of the silica core was obtained using a boiling Murakami solution. The dissolution of the SiO_2 through pores present in the coating is expected, as seen on Figure 6. Dissolved silica particles revealed a crack on coating corresponding to either uncoated part of silica during the MPCVD growth or a fragment detached during sonication step. This last step is required to separate coated particles which coalesced during the growth.

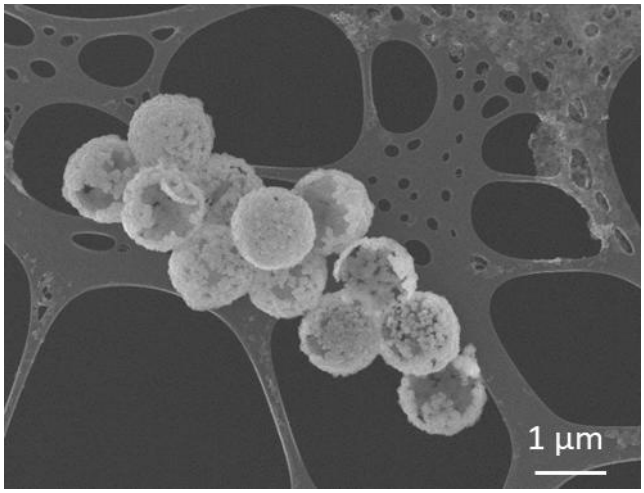

Figure 6 : SEM image of shells obtained after silica etching.

FTIR spectroscopy further confirmed the complete etching of silica cores and the presence of different functional groups at the surface of shells (Figure 9). Silica particles present their main absorption peaks at 800 cm^{-1} and 1105 cm^{-1}, assigned to the Si-O-Si bending vibration and asymmetric stretching vibrations, respectively[27]. The weak line at about 960 cm^{-1} is ascribed to the asymmetric bending and stretching vibrations of Si-OH silanol functional groups. The IR band at 3437 cm^{-1} is assigned to the stretching vibrations of strongly adsorbed H_2O molecules while the one at 1632 cm^{-1} corresponds to the bending vibration of these H_2O molecules [28], [29], [29].

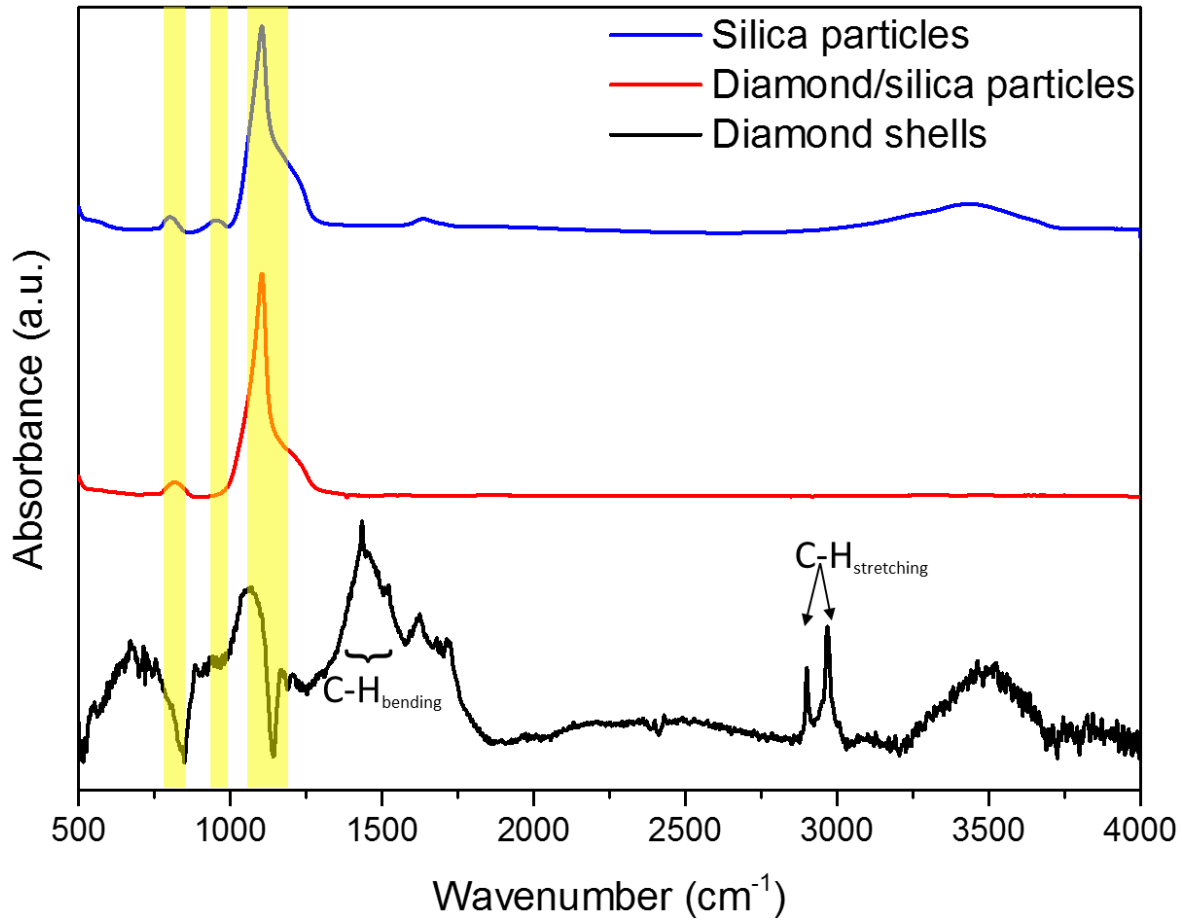

Figure 7 : Transmission FTIR spectra of silica particles, coated silica particles and shells dried for 4h under a dry N_2 flow at room temperature. The higher level of noise in the shells spectrum is due to the very limited amount of material present in the KBr pellet.

After MPCVD growth, all peaks related to Si-OH and water are not visible, confirming surface modifications induced by the MPCVD plasma at silica surface. After dissolution of the silica cores, a vanishing of the characteristic peaks observed for silica particles is observed, confirming their removal.

The FTIR spectrum of shells also revealed the signature of C-H peaks at 2916 cm^{-1} and 2850 cm^{-1} and close to 1400 cm^{-1} corresponding to C-H stretching and C-H bending, respectively [24]. These C-H bonds can be ascribed to grain boundaries in the nanocrystalline structure. The shoulder between 1630 cm^{-1} and 1800 cm^{-1} can be reasonably attributed to C=O stretching band, in agreement with the surface oxidation of the coating [31].

The crystalline structure of the hollow spheres synthesized at 2 % of methane for 10 min was then investigated by HR-TEM. The coating is composed of diamond crystallites with sizes ranging up to 20 nm (Figure 10a), confirming the growing of diamond by MPCVD from the nanodiamonds seeds of 5 nm. The inversed Fast Fourier Transform (FFT) image allows to measure the interplanar distance of 0.2 nm characteristic of (111) diamond planes within these crystals. No organized graphitic structures could be clearly distinguished on this figure. However, amorphous carbon areas have been observed coexisting with diamond crystallites.

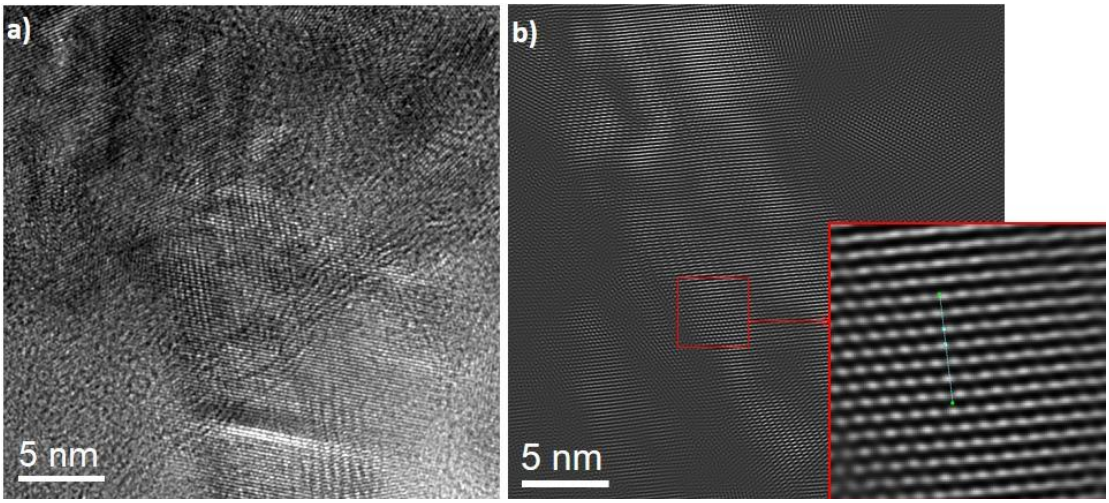

Figure 8 : HR-TEM micrograph of a) hollow diamond spheres synthesized at 2 % of methane during 10 min b) Inversed FFT signal of the area shown in a) with an inset showing the measurement of the interplanar distance.

Diamond shells were then dispersed in water. The DLS characterizations are provided in Figure 9 and compared with silica particles before and after coating. The hydrodynamic diameter exhibits a principal peak at 1127 nm assigned to isolated hollow spheres and a second weaker peak at 5279 nm corresponding to a limited amount of aggregated spheres. A third peak appears at 128 nm which likely represents a population of coating fragments broken during the sonication process. The main diameter values compare well with the one measured for the aqueous suspension of coated silica particles (Figure 9). This proves the robustness of the coating after the chemical and sonication treatments. The Zeta potential of diamond hollow spheres remains negative, with a value of -47 mV similar to the one of coated silica particles.

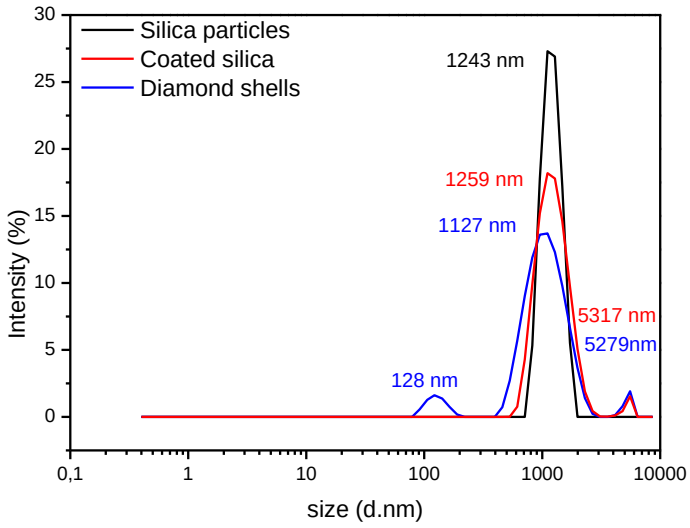

Figure 9 : Hydrodynamic diameter distributions of as received silica particles (in black), oxidized diamond coated silica particles (in red) and diamond shell (blue) in water suspension.

3.3 Tuning of crystalline structure of coatings

SEM images of coated silica particles synthesized with different methane/hydrogen ratios are shown in Figure 10.

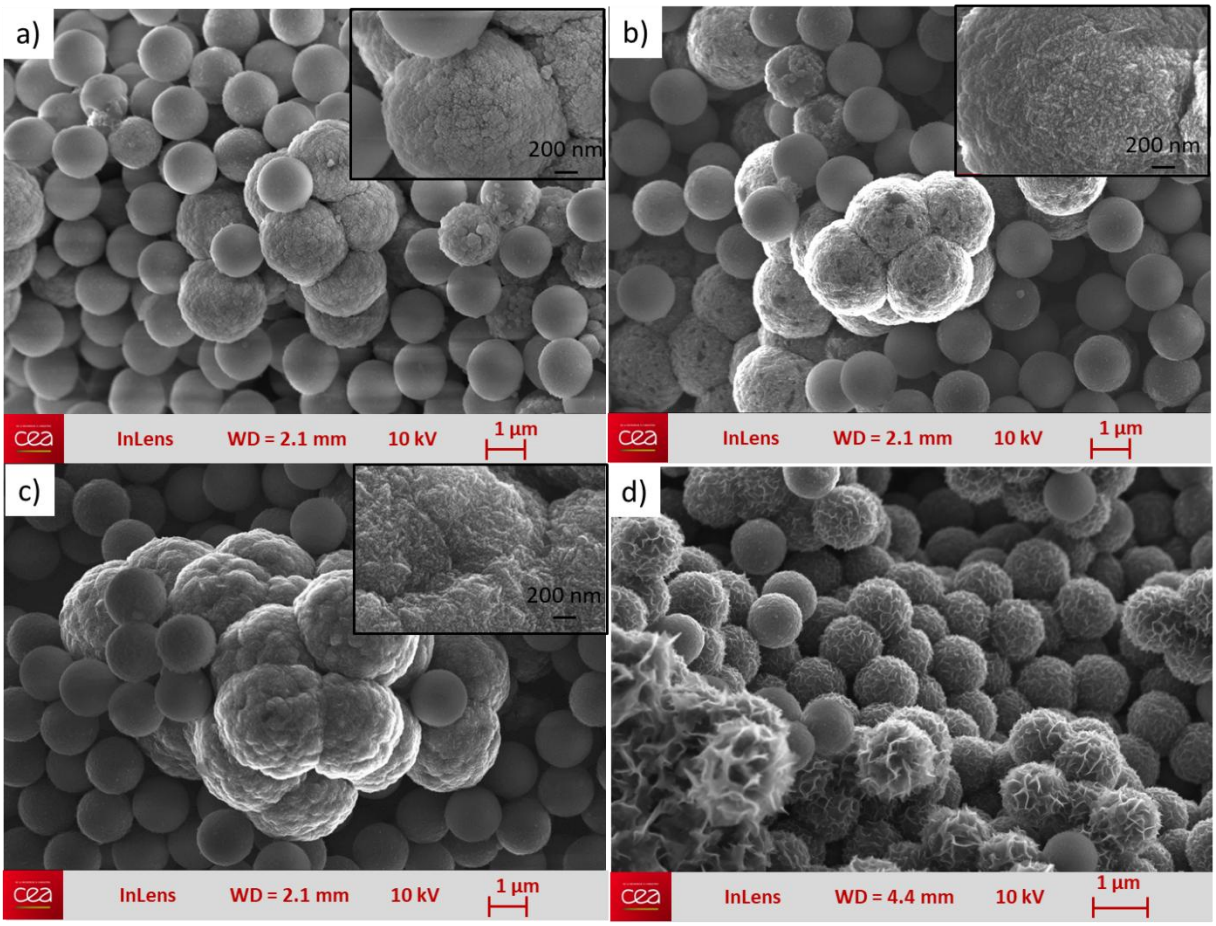

Figure 10 : Evolution of the surface morphology of silica particles seeded with NDs after MPCVD growth for different methane/hydrogen ratio a) 2%, b) 5%, c) 10 % and d) 30 %. Other MPCVD

parameters: total pressure 12.5 mbar, flow rate 10 sccm, microwave power 180 W, deposition time 1 hour, for the highest methane content (30 %) it was reduced to 45 min.

SEM images allow a first evaluation of the effect of the methane concentration on the coating morphology (Figure 12). It appears that this morphology remains rather similar. The average grain size does not significantly evolve except when methane concentration rises to 30%. Nevertheless, as expected, the increase of methane/hydrogen ratio strongly influences the growth rate, at least for the three lowest methane ratios. First estimations of the average diameter of the particles correspond to growth rates of 0.3 µm/h, 0.4 µm/h and 0.5 µm/h for methane content of 2%, 5% and 10%, respectively. The growth rate slows down at higher % CH_4. This behavior can be attributed to the higher concentration of carbon radicals present in the plasma which saturate the surface of particles in carbon radical species. A similar trend was previously reported for growth of conventional diamond films on silicon substrates [32,33]. For 30% methane concentration, a particular morphology was observed (Figure 10d) which is similar to the one previously reported by Lee at al. for graphite materials called graphite nanoflakes [19]. Note that as for 2% methane ratio, uncoated silica particles remain in the sample, due to the geometry of the MPCVD reactor.

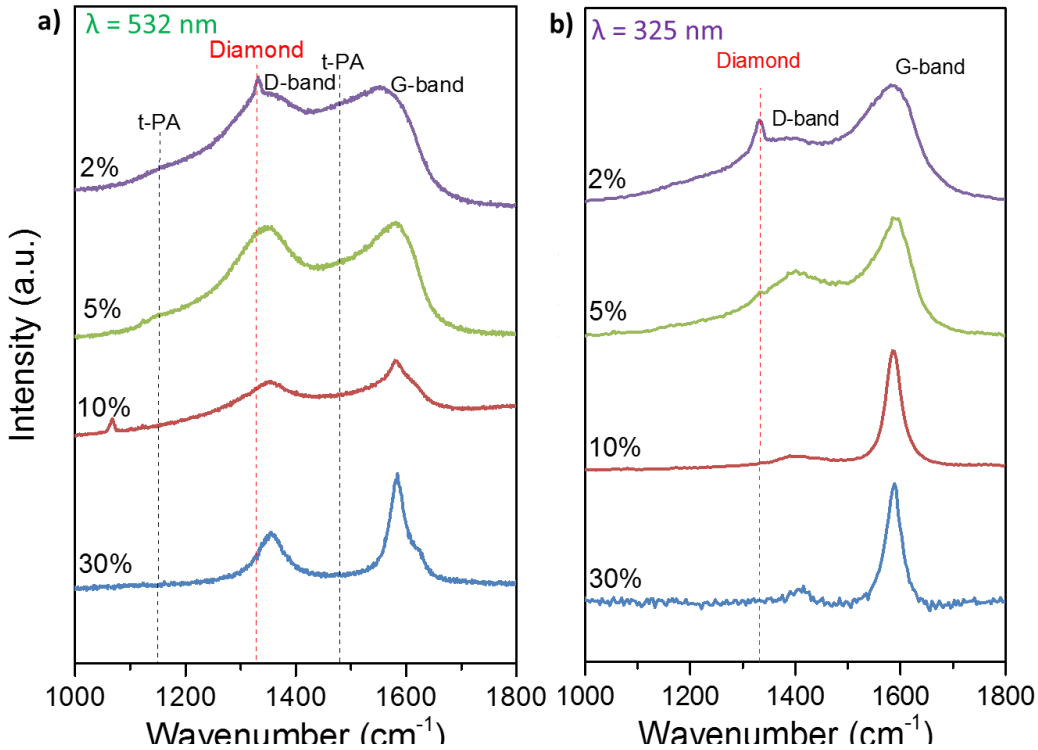

Figure 11 : a) Visible (λ=532 nm) and b) UV (λ=325) Raman spectra of coatings grown on silica particles with different methane contents: 2 %, 5 %, 10 % and 30 %.

The Raman spectra recorded with visible (532 nm) and UV (325 nm) wavelengths are provided on Figure 11. To increase the quality of the measurements, experiments were performed on diamond shells, i.e. after dissolution of silica cores. As expected, the Raman spectra demonstrate the strong effect of the methane content on the crystalline quality of the coating. For the lowest methane concentration (2 %), the visible Raman spectra exactly correspond to those already reported and well documented of nanocrystalline CVD films [34]. Here, the diamond line located at 1332 cm^{-1} is observable, accompanied with broad lines with maxima at about 1150, 1350, 1480 and 1580 cm^{-1}. The 1350 and 1580 cm^{-1} correspond to the so-called “D” and “G” lines of defective graphite, while

the 1150 and 1480 cm^{-1} lines track the presence of trans-polyacetylene (t-PA) within the grain boundaries.

For higher methane contents, the “D” and “G” lines are the main observable features, without any clear evidence of the presence of diamond in the coatings. When the methane content is raised up to 30%, the spectra indicate a high graphite crystallinity, as judged from the low “D”/”G” intensity ratio and the narrower line widths of “D” and “G” lines. Tuning the excitation wavelength to 325 nm, the same trends are still observed. However, diamond is observed for the samples grown for methane concentrations of 2 and 5%, and disordered graphite is clearly evidenced for all the samples. According to previous report, the effect of higher methane concentration (between 10 and 20 %) lowers the grain size of the nanocrystalline structure promoting secondary nucleation [35]. Because of the double resonance process specific to graphitic materials, the “D” line is now peaking at about 1400 cm^{-1}, and its intensity is somehow quenched as compared to usual excitations in the visible spectral range. A small variability of the spectra for all the samples has been noted. However, this does not call into question the observed trends. Thus, as more or less expected, the Raman spectra of samples indicate that low methane concentration promote the growth of diamond films, while the use of higher methane contents (10% and more) leads to the formation of graphite flakes. Finally, similar results were obtained on the core-shell silica-diamond coated particles by P. John [19].

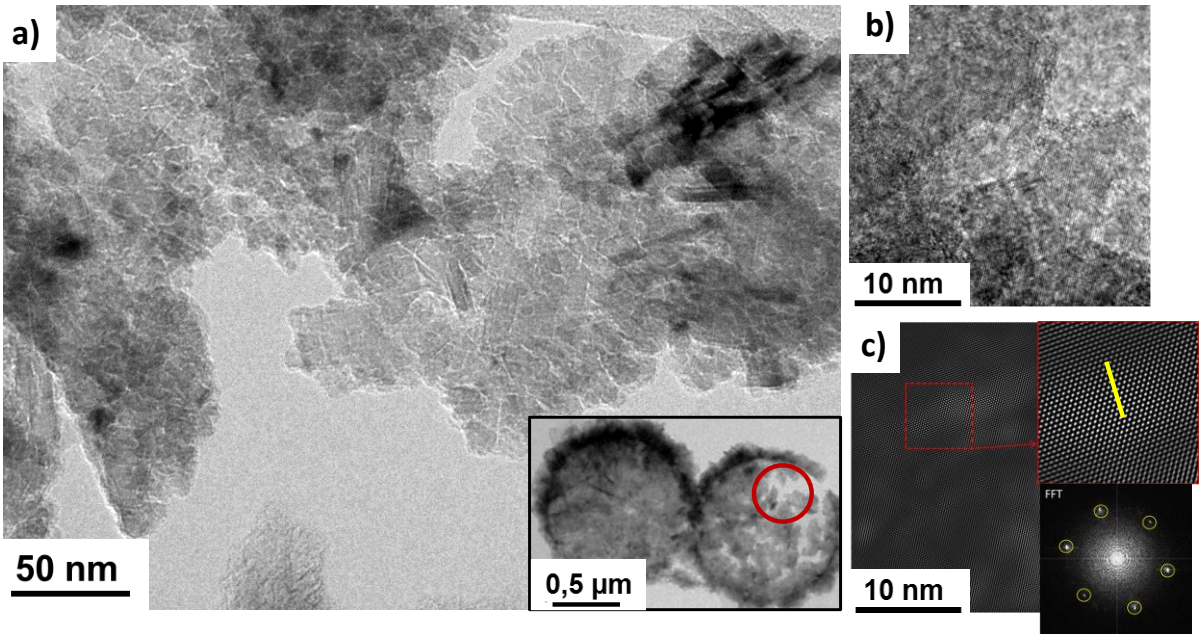

Figure 12 : a) HR-TEM image of a diamond shell grown at 2% of methane during 1 hour (inset) and its nanocrystalline structure b) HR-TEM image of several diamond crystals c) Inversed FFT signal of the area shown in b) with an inset showing the measurement of the interplanar distance, 0.2 nm, in agreement with diamond (111) planes.

The Raman spectrum of the sample synthesized with 2% of methane was superimposed on a huge photoluminescence (PL) background (shown in Figure 13). Examining this room temperature PL background in the 515 – 800 nm spectral range, clear signatures of the $[N\text{-}V]^0$ and $[N\text{-}V]^-$ color centers at about 575 nm and 637 nm were observed with their respective phonon side bands. Here, the presence of nitrogen in the diamond lattice is due to small leaks in the deposition set-up at seals of the quartz tube. In fact, Optical Emission Spectroscopy (OES) showed the presence of nitrogen species in the MPCVD plasma (data not shown). On the other hand, and more surprisingly, spectra gave no evidence of [Si-V] centers (expected at 738 nm), often observed when growth chambers include silica tubes or that could be expected from a partial etching of the silica particles at the

beginning of the growth process. Nevertheless, no intentional post treatments were applied here, as annealing for instance, to promote the formation of colored centers.

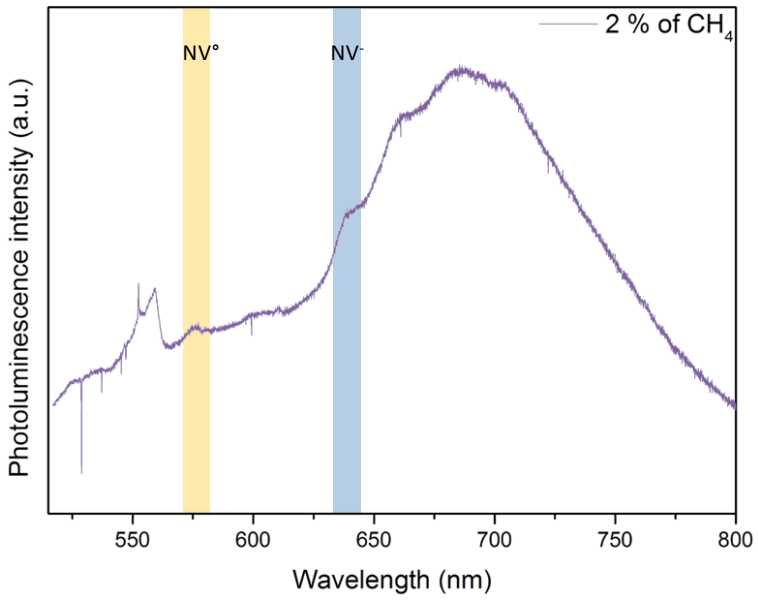

Figure 13 : Photoluminescence spectra obtained on diamond coating synthesized at 2 % of methane using an excitation at 514 nm.

Coatings grown at 2% and 30% of methane were also investigated by HR-TEM after a dissolution of silica cores (Figure 12 and Figure 14). As for samples grown for 10 min with 2 % of methane (presented in Figure 8), the coating obtained after 1h of growth exhibits faceted crystals bigger than 20 nm meaning that the growth took place from the NDs seeds of 5 nm. From the inversed Fast Fourier Transform (FFT) image, an interplanar distance of 0.2 nm characteristic of (111) diamond planes was measured (Figure 14c). No organized graphitic structures could be clearly distinguished.

For a hollow sphere grown at 30 % of methane, two different zones are presented in Figure 14. In the first zone, diamond is not evidenced (Figure 16a). The inversed FFT image revealed interplanar distances of 0.37 nm corresponding to (002) planes of graphite (Figure 16b and insert). These observations well support the Raman spectra previously discussed (Figure 13). Within the second zone, the same graphitic planes have been found (Figure 16c). Nevertheless, the inversed FFT image also showed the presence of diamond crystals of few nm (Figure 16d and insert) with an interplanar distance of 0.2 nm, in well agreement with (111) diamond planes. These HR-TEM observations suggest that initial diamond seeds are preserved after the MPCVD growth at 30% of methane. These seeds are embedded in a graphitic structure very similar to graphite nanoflakes.

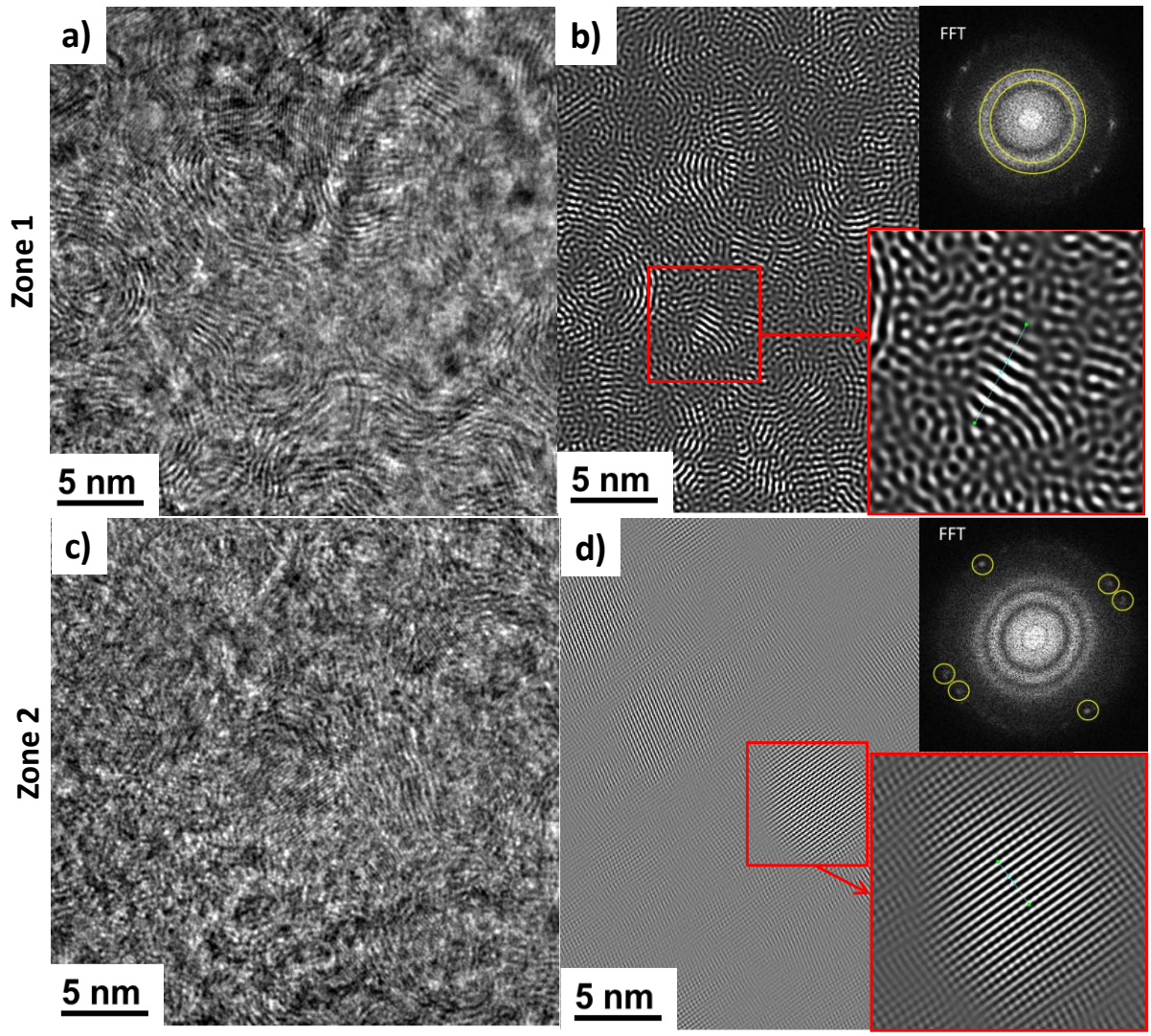

Figure 14 : HR-TEM micrographs of a hollow sphere grown at 30 % of methane during 45 min in two different regions zone 1: a) HR-TEM micrographs b) FFT and inversed FTT image with an insert showing the measured interplanar distances. zone 2: c) HR-TEM micrographs d) FFT and inversed FTT image with an insert showing the measured interplanar distances.

Finally, colloidal properties of nanoflake particles grown during 15 min at 30% of methane were investigated by DLS and compared to initial silica particles dispersed in aqueous suspension (Figure 17). This growth time was optimized to obtain spherical graphite nanoflakes. These particles underwent first the UV/ozone surface treatment to render them hydrophilic. According to DLS, the well-defined size distribution is preserved after the MPCVD growth. The zeta potential at -57mV is significantly negative meaning that the colloidal suspensions is stable.

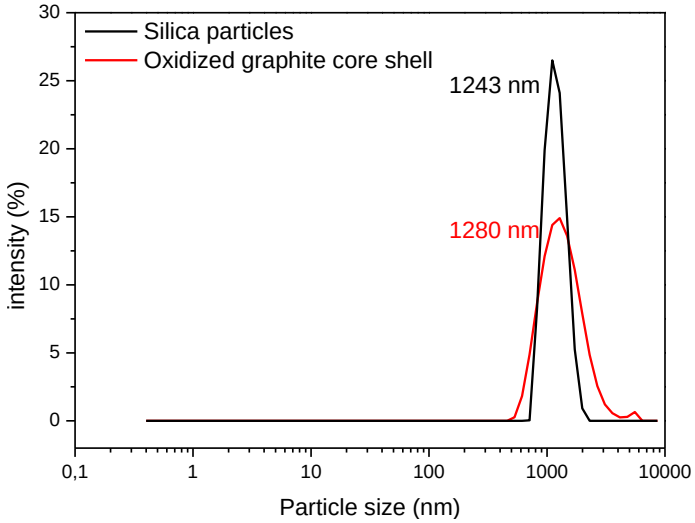

Figure 15 : Distributions of the hydrodynamic diameter for as received silica particles (in black) and oxidized graphite nanoflakes grown during 15 min on silica particles (in red) with ZP= -57 mV.

The formation of self-assembly building blocks onto a silicon wafer substrate was observed by FE-SEM (Figure 16a) with hexagonal arrangement in domains up to 50 µm (inset Figure 16a). This behavior is related to the narrow size distribution and the spherical shape of the coated particles. Such structures can be of interest for fabrication of photonic crystals. By dissolving the silica core, graphite nanoflakes shells were obtained (Figure 16b). From FE-SEM images, the coating thickness was estimated to 20-50nm.

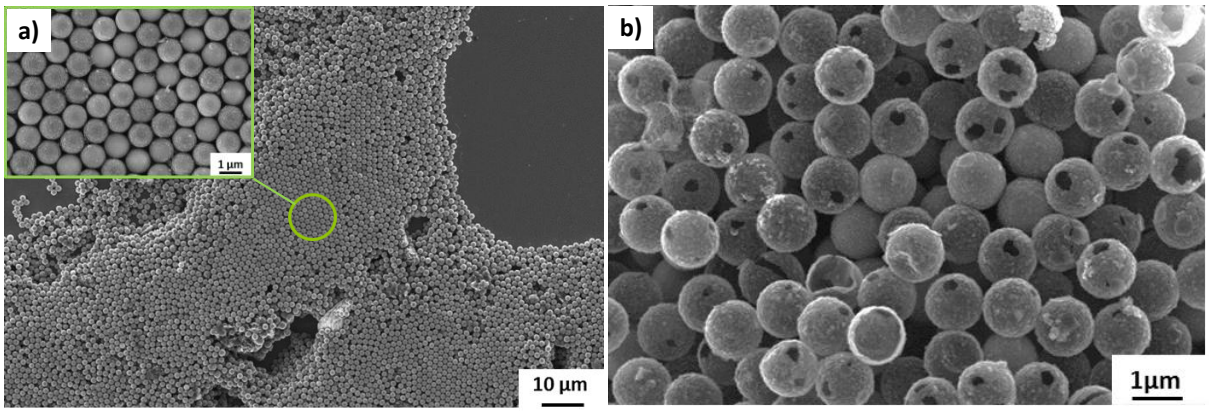

Figure 16 : a) FE-SEM images of self-assembly of graphite nanoflakes coated particles deposited on silicon substrate exhibiting a hexagonal structure. Other MPCVD parameters: total pressure 12.5 mbar, flow rate 10 sccm, microwave power 180 W, 30 % of methane during 15 minutes. b) FE-SEM image of graphite nanoflakes shells obtained after a dissolution of silica core by basic solution.

4. Conclusions

The present study reports on a new approach to create monodispersed diamond core-shells particles dispersible in water. Based on a template of silica particles, the synthesis was performed with a microwave plasma CVD reactor specifically designed for powder treatments. The seeding of silica particles with nanodiamonds was first accurately adjusted to get an optimal seeds density with a

strong adherence. A nanocrystalline diamond coating was characterized by Raman and HR-TEM after a MPCVD growth using 2 and 5% of methane in hydrogen. According to PL spectra recorded by Raman, neutral and negatively charged [N-V] centers are present within this diamond coating. Furthermore, after 10 min of diamond growth and a sorting of particles, an oxidation treatment allowed to obtain monodispersed diamond core-shells stable in aqueous suspension. The silica template can then be removed using a simple wet chemical etching process as confirmed by FTIR, to obtain diamond hollow shells which also showed excellent stability in aqueous suspension with a narrow size distribution in DLS. This material exhibits a significant increase of specific surface area compared to coated particles.

This approach revealed to be highly versatile to tune the crystalline structure of the deposited carbon material. Indeed, by using higher methane content up to 30%, graphite nanoflakes were formed and observed by Raman, HR-TEM and FE-SEM. HR-TEM revealed that initial diamond seeds are embedded within a graphitic matrix. These particles were found to be also stable in aqueous suspension. Their spherical shape allowed the deposition of self-assembled layers on silicon substrates exhibiting a hexagonal-type symmetry which may promising for fabrication of photonic crystals.

This work reports on the synthesis of a new class of diamond-based material, made of spherical and monodispersed objects. These results open new perspectives for diamond material to catalyst supports, adsorbents, gas storage, electrodes and fuel cells [36]. As color centers can be hosted by diamond core-shells, this material may also have applications in the field of biomedicine for diagnosis and therapy where the biocompatibility and the carbon surface chemistry of diamond are major assets.

Acknowledgement

A.V. thanks DIACAT for PhD funding. This project has received funding from the European Union's Horizon 2020 Program under Grant Agreement No. 665085 (DIACAT).

References and notes

[1] V. N. Mochalin, O. Shenderova, D. Ho, Y. Gogotsi, *Nat Nano* **2012**, *7*, 11.
[2] J.-P. Boudou, P. A. Curmi, F. Jelezko, J. Wrachtrup, P. Aubert, Mohamed Sennour, G. Balasubramanian, R. Reuter, A. Thorel, E. Gaffet, *Nanotechnology* **2009**, *20*, 235602.
[3] N. Mohan, C.-S. Chen, H.-H. Hsieh, Y.-C. Wu, H.-C. Chang, *Nano Letters* **2010**, *10*, 3692.
[4] J.-C. Arnault, *Nanodiamonds: Advanced Material Analysis, Properties and Applications*, William Andrew, **2017**.
[5] M. Ozawa, M. Inaguma, M. Takahashi, F. Kataoka, A. Krüger, E. Ōsawa, *Adv. Mater.* **2007**, *19*, 1201.
[6] A. Krueger, D. Lang, *Adv. Funct. Mater.* **2012**, *22*, 890.
[7] V. N. Mochalin, I. Neitzel, B. J. M. Etzold, A. Peterson, G. Palmese, Y. Gogotsi, *ACS Nano* **2011**, *5*, 7494.
[8] R. Schirhagl, K. Chang, M. Loretz, C. L. Degen, *Annual Review of Physical Chemistry* **2014**, *65*, 83.
[9] V. Chakrapani, J. C. Angus, A. B. Anderson, S. D. Wolter, B. R. Stoner, G. U. Sumanasekera, *Science* **2007**, *318*, 1424.
[10] A. Pentecost, S. Gour, V. Mochalin, I. Knoke, Y. Gogotsi, *ACS Applied Materials & Interfaces* **2010**, *2*, 3289.
[11] I. Rehor, P. Cigler, *Diamond and Related Materials* **2014**, *46*, 21.
[12] Z. Chu, S. Zhang, B. Zhang, C. Zhang, C.-Y. Fang, I. Rehor, P. Cigler, H.-C. Chang, G. Lin, R. Liu, Q. Li, *Scientific Reports* **2014**, *4*, 4495.

[13] J. Havlik, V. Petrakova, I. Rehor, V. Petrak, M. Gulka, J. Stursa, J. Kucka, J. Ralis, T. Rendler, S.-Y. Lee, R. Reuter, J. Wrachtrup, M. Ledvina, M. Nesladek, P. Cigler, *Nanoscale* **2013**, *5*, 3208.
[14] M. Maas, T. Bollhorst, R. N. Zare, K. Rezwan, *Part. Part. Syst. Charact.* **2014**, *31*, 1067.
[15] Q. Wang, J. Bai, B. Dai, Z. Yang, S. Guo, L. Yang, Y. He, J. Han, J. Zhu, *Chemical Communications* **2017**, *53*, 2355.
[16] Z. N. Tetana, S. D. Mhlanga, N. J. Coville, *Diamond and Related Materials* **2017**, *74*, 70.
[17] Z. Xue, J. C. Vinci, L. A. Colon, *ACS Appl. Mater. Interfaces* **2016**, DOI 10.1021/acsami.5b11871.
[18] J.-K. Lee, M. W. Anderson, F. A. Gray, P. John, *Diamond and Related Materials* **2007**, *16*, 701.
[19] J.-K. Lee, P. John, *Thin Solid Films* **2010**, *519*, 625.
[20] F. Gao, M. T. Wolfer, C. E. Nebel, *Carbon* **2014**, *80*, 833.
[21] J. C. Arnault, H. A. Girard, in *Nanodiamond*, **2014**, pp. 221–252.
[22] H. A. Girard, S. Perruchas, C. Gesset, M. Chaigneau, L. Vieille, J.-C. Arnault, P. Bergonzo, J.-P. Boilot, T. Gacoin, *ACS Applied Materials & Interfaces* **2009**, *1*, 2738.
[23] J. C. Arnault, H. A. Girard, *Current Opinion in Solid State and Materials Science* **2016**, DOI 10.1016/j.cossms.2016.06.007.
[24] H. A. Girard, J. C. Arnault, S. Perruchas, S. Saada, T. Gacoin, J.-P. Boilot, P. Bergonzo, *Diamond and Related Materials* **2010**, *19*, 1117.
[25] H. A. Girard, T. Petit, S. Perruchas, T. Gacoin, C. Gesset, J. C. Arnault, P. Bergonzo, *Physical Chemistry Chemical Physics* **2011**, *13*, 11517.
[26] R. Boukherroub, X. Wallart, S. Szunerits, B. Marcus, P. Bouvier, M. Mermoux, *Electrochemistry Communications* **2005**, *7*, 937.
[27] T. López, J. L. Bata-García, D. Esquivel, E. Ortiz-Islas, R. Gonzalez, J. Ascencio, P. Quintana, G. Oskam, F. J. Álvarez-Cervera, F. J. Heredia-López, J. L. Góngora-Alfaro, *Int J Nanomedicine* **2011**, *6*, 19.
[28] G. Dingemans, C. A. A. van Helvoirt, D. Pierreux, W. Keuning, W. M. M. Kessels, *J. Electrochem. Soc.* **2012**, *159*, H277.
[29] S. C. Feifel, F. Lisdat, *Journal of Nanobiotechnology* **2011**, *9*, 59.
[30] C. Jiang, Y. Zhang, Q. Wang, T. Wang, *Journal of Applied Polymer Science* **2013**, *129*, 2959.
[31] T. Petit, L. Puskar, T. Dolenko, S. Choudhury, E. Ritter, S. Burikov, K. Laptinskiy, Q. Brzustowski, U. Schade, H. Yuzawa, M. Nagasaka, N. Kosugi, M. Kurzyp, A. Venerosy, H. Girard, J.-C. Arnault, E. Osawa, N. Nunn, O. Shenderova, E. F. Aziz, *J. Phys. Chem. C* **2017**, *121*, 5185.
[32] S. Matsumoto, Y. Sato, M. Tsutsumi, N. Setaka, *Journal of Materials Science* **1982**, *17*, 3106.
[33] A. Gicquel, K. Hassouni, F. Silva, J. Achard, *Current Applied Physics* **2001**, *1*, 479.
[34] J. Birrell, J. E. Gerbi, O. Auciello, J. M. Gibson, J. Johnson, J. A. Carlisle, *Diamond and Related Materials* **2005**, *14*, 86.
[35] S. Saada, J. C. Arnault, L. Rocha, B. Bazin, P. Bergonzo, *physica status solidi (a)* **2008**, *205*, 2121.
[36] S. Li, A. Pasc, V. Fierro, A. Celzard, *J. Mater. Chem. A* **2016**, *4*, 12686.